Journal of Materials Chemistry B

ROYAL SOCIETY OF CHEMISTRY

PAPER

View Article Online
View Journal | View Issue

Check for updates

Cite this: J. Mater. Chem. B, 2025, 13, 6804

Iron(II)-catalysed tyrosinase crosslinked hyaluronic acid hydrogel for the controlled release of human antibodies†

Seth Asamoah, *[ab] Martin Pravda,*[b] Jana Matonohová, [b] Tereza Bártová,[b] Eva Šnejdrová, [a] Sebastian Spiegel, [cdef] Andrew Chan,[cde] Vincent Pernet [cdegh] and Vladimír Velebný[b]

Received 21st November 2024,
Accepted 27th March 2025

DOI: 10.1039/d4tb02606c

rsc.li/materials-b

Tyrosinase is a common crosslinker used in the formation of in situ hydrogels, often resulting in significantly longer gelation times. The rate-determining step for the interconversion between the four discrete states of the enzyme is characterized by a lag phase, which contributes to its slow gelation kinetics. In this study, we report, for the first time, the use of a catalytic amount of iron(II) to produce fast in situ-gellable tyramine-conjugated hyaluronic acid hydrogels (HATA), which are prospectively applicable for nasal drug delivery. We observed gelation times ranging from 886 to 538 seconds, depending on the polymer and enzyme concentrations, irrespective of the pH level tested. The presence of iron(II) significantly reduced the gelation time by an order of magnitude, ranging from 86 seconds to 25.46 seconds, depending on the polymer concentration, pH, and enzyme activity. Based on our findings, we propose a double crosslinking mechanism involving catechol–catechol coupling and catechol–iron(II) complex formation, as evidenced by improvements in the rheological properties of the hydrogels. These novel hydrogels can encapsulate antibodies and provide prolonged release for up to two weeks. Additionally, we confirmed that the crosslinking chemistry did not affect the bioactivity of the antibodies. Given their improved mucoadhesive properties, we envision these hydrogels as promising candidates for the formulation of bioadhesive drug delivery systems.

1 Introduction

Antibody based therapies have been on the rise in recent times due to their capacity to outmatch small molecule drugs in terms of their targeted mode of action and reduction of undesired effects.[1] In 2023, about 200 of these antibody loaded formulations were granted market approval or were considered by regulatory authorities in at least one country.[2] Antibodies have high binding affinity and minimal side effects, making them a suitable alternative to small-molecule drugs with the same therapeutic action.[2,3] They have been employed in the treatment of a wide range of diseases including cancers,[4] eye macular degeneration, hypertension and thromboembolic diseases, just to highlight a few.[5] While antibodies have been administered directly without any carrier in the past, polymer carriers have recently been used to deliver antibody therapies.[6–8] Pioneers in the development of hydrogels as carriers for antibodies in drug delivery applications used poly(ethylene-*co*-vinyl acetate) for the sustained release of antibodies.[9] One study used hyaluronic acid as an anchor to tether the Nogo-66 receptor antibody and poly-L-lysine to promote axonal regeneration post-spinal cord injury.[10] Another study also loaded the anti-Nogo-A antibody in poly(lactic-*co*-glycolic acid) nanoparticles into a composite hydrogel of methylcellulose and hyaluronan for the therapy of spinal cord injury.[11] The hydrogels mentioned above have mostly been produced using complex procedures or harsh chemical solvents, which could potentially affect antibody efficiency as well as the environment.[9,11] As an alternative,

[a] Department of Pharmaceutical Technology, Faculty of Pharmacy, Charles University, Akademika Heyrovského 1203/8, 500 03 Hradec Králové 3, Czech Republic
[b] Contipro a.s., Dolní Dobrouč 401, 56102, Dolní Dobrouč, Czech Republic
[c] Department of Neurology, Inselspital, Bern University Hospital, University of Bern, 3010 Bern, Switzerland
[d] Experimental Neurology Center (ZEN), Bern University Hospital, University of Bern, 3010 Bern, Switzerland
[e] Department of Biomedical Research, University of Bern, 3010 Bern, Switzerland
[f] Graduate School for Cellular and Biomedical Sciences, University of Bern, 3010 Bern, Switzerland
[g] Department of Molecular Medicine, Faculty of Medicine, Laval University, Quebec City, Qc, Canada
[h] Centre de Recherche du CHU de Québec - Université Laval, Axe Médecine Régénératrice, Québec, Québec City, Canada

† Electronic supplementary information (ESI) available. See DOI: https://doi.org/10.1039/d4tb02606c

enzymatic methods of crosslinking have been explored, but so far minimally.[6]

Enzymatic crosslinking has been used as a method to produce 3-dimensional hydrogel materials.[12–14] It is advantageous owing to its ability to proceed under mild physiological conditions. Enzyme-mediated crosslinking is noted for its high substrate specificity, which helps avoid unwanted side reactions typically associated with chemical crosslinking or photocrosslinking methods.[15] Common enzymes employed in producing hydrogels include transglutaminase, phosphopantetheinyl transferase, horseradish peroxidase, tyrosinase, sortase, and alkaline phosphatase, among others.[16,17]

Oxidoreductase enzymes such as tyrosinase or horseradish peroxidase are the most common crosslinking enzymes for hydrogels production. Earlier studies have used tyrosinase directly to oxidize the tyrosyl moieties of gelatine, followed by non-enzymatic crosslinking with amine-rich polymers such as chitosan.[18]

Generally, polymers intended to be crosslinked by these two oxidoreductase enzymes are chemically modified to incorporate phenolic groups which act as substrate to facilitate its crosslinking.[19] To directly crosslink gelatine without the need for other polymer additives a recombinant tyrosinase was developed by Kim *et al.* to improve upon the gelation kinetics, crosslink density and mechanical properties of the hydrogels.[20] Also, tyrosinase has an advantage which stems from its use of molecular oxygen as a co-substrate which produces water as by-product unlike like horseradish peroxidase which uses hydrogen peroxide as a co-substrate which could be potentially toxic to cells.[15] Coupled with these advantages is the ability of tyrosinase to oxidize its substrates into mussel-like adhesive foot proteins, which have the capacity to bind strongly and thrive in moist environments through the formation of hydrogen bonds, metal coupling, and effective covalent crosslinks. Tyrosinase is considered safe and is used to produce surgical adhesives as an alternative to conventional ones such as fibrin glue and cyanoacrylate.[13,21] Tyrosinase crosslinked hydrogels are also known to prolong the contact time at mucosal surfaces making them desirable for mucoadhesive applications.[22,23]

Tyrosinase is an enzyme that contains copper and aids in the tyrosine and other phenol containing compound's conversion into L-3,4-dihydroxyphenylalanine (L-DOPA), and then further oxidizes dopa into dopaquinone. The initial hydroxylation step, which is the slowest and controls the overall kinetics of melanin production in mammals and plants, possesses a significant lag phase. This delay happens because the enzyme undergoes hysteresis, which affects its activity over time. Factors such as pH, nature of substrate, an appropriate hydrogen donor and enzyme concentration affects the lag phase of the enzyme.[24]

In terms of using this enzyme to crosslink hydrogels, it has led to significantly longer gelation times in the order of minutes which makes it unsuitable for *in situ* crosslinking or other applications that requires the rapid curing of the hydrogels. Particularly in developing *in situ* hydrogels for nasal applications, a rapid sol–gel transition is desired due to its several advantages. This rapid gelation prolongs the resident time of the formulation by establishing an immediate contact with the nasal mucosa. This feature ensures optimal bioavailability while minimizing mucociliary clearance.[25] Rapid gelation also mitigates patient discomfort by reducing the residence time of liquid formulations in their nasal cavity ensuring patient compliance.[25,26] It also prevents dripping and leakage of formulations which could potentially lead to underdosing.[25] To overcome tyrosinase's slow gelation kinetics some formulators have resorted to using higher enzyme concentrations or by combining it with other enzymes such as horseradish peroxidase.[12,27] Palumbo and co-workers first investigated the effects of metal ions on the kinetics of oxidation of tyrosine catalysed by tyrosinase. They reported that catalytic amount of various cations influenced the kinetic properties of tyrosinase. Among them, iron(III) and iron(II) were also investigated with minimal influence on the kinetic properties by iron(III). However, iron(II) had the same effect as dopa in substantially stimulating the tyrosine hydroxylase activity of the enzyme.[28]

Capitalizing on this phenomenon, we are reporting for the first time the synthesis of tyramine functionalized hyaluronic acid hydrogels with tyrosinase in the presence of catalytic amount of iron(II). The presence of the iron(II) in the hydrogels significantly improved the kinetics of gelation of hydrogels by an order of a magnitude rendering it suitable for *in situ* nasal applications. The hydrogels produced were also used as drug delivery device for the controlled release of Privigen®. Privigen® is an immune intravenous human globulin for the treatment of primary humoral immunodeficiency (PI), Chronic immune thrombocytopenic purpura (ITP) and Chronic inflammatory demyelinating polyneuropathy (CIDP).[29] We have also extensively characterized these new hydrogels in terms of their rheological properties, rate of degradation, swelling properties, mesh size, crosslinking density, catechol conversion and its coupling products stemming from hydrogel formation, iron(II)–catechol complexes, mucoadhesiveness and finally it's *in vitro* cytotoxicity on NIH/3T3 fibroblasts.

2 Materials and methods

2.1 Materials

Tyrosinase from mushroom-lyophilized powder, ≥1000 unit per mg solid, rhodamine B isothiocyanate-mixed isomers, hyaluronidase from bovine testes type I-S, lyophilised powder, 400–1000 units per mg solid, iron(II) sulphate heptahydrate and procine gastric mucin type II were purchased from Sigma Aldrich, St. Louis, United States. Hyaluronic acid tyramine derivative with a degree of substitution 6.5% (HATA) (1 MDa) was obtained from Contipro a.s. Dolni Dobrouc, Czech Republic. Potassium dihydrogen phosphate and sodium acetate were purchased from Lach-Ner s.r.o, Czech Republic. Sodium chloride, Sodium phosphate dibasic dodecahydrate and potassium chloride were purchased from Penta Chemicals in the Czech Republic. Privigen® was received as a gift from Bern University Hospital-Inselspital.

2.2 Methods

2.2.1 Polymer synthesis and kinetics of gelation. The synthesis of the tyramine derivative of hyaluronic acid has previously been described thoroughly in our paper.[30] The degree of substitution of tyramine was determined to be 6.5% using ^{1}HNMR and the molecular weight was determined with size exclusion chromatography coupled with multi angle laser light scattering (SEC-MALLS). The molecular weight and polydispersity index were 1 000 000 and 1.5 respectively.

The polymer concentration, pH, enzyme concentration and the presence of iron(II) was probed for its influence on the gelation time of the hydrogels. Briefly 1 and 2% w/v HATA were dissolved in acetate buffer (pH 5.6 or 6.5 within the pH range of the nasal cavity[31] adjusted using acetic acid or NaOH) for three hours at 60 °C and left to completely dissolve overnight at room temperature. To evaluate the gelation time, tyrosinase concentrations of 1.25 kU mL^{-1}, 2.5 kU mL^{-1}, or 5 kU mL^{-1} were added to an equal volume of HATA in a vial and stirred at 300 RPM at room temperature until the stirrer came to a complete stop, with the time recorded as the gelation time. The final tyrosinase concentration was 0.625 kU mL^{-1}, 1.25 kU mL^{-1} or 2.5 kU mL^{-1} and the HATA concentration was 0.5 or 1% w/v. These set of hydrogels served as a control. To test the influence of the iron(II) on the gelation time, tyrosinase was homogeneously mixed with iron(II) in acetate buffer. Whiles HATA pH remained constant after dissolution, the pH after mixing the enzyme and iron(II) dropped to 6 due to hydrolysis of iron(II)[32] which was later adjusted with NaOH or acetic acid to pH 5.6 or 6.5 within the pH range of the nasal cavity.[31] The mechanism of crosslinking is shown schematically in Fig. 1. The resulting precursor solution was then mixed with HATA and stirred on a magnetic stirrer until the stirring bar came to a complete stop. The final concentration of iron(II) was 0.9 mM or 1.8 mM and tyrosinase final concentration was 0.625 kU mL^{-1}, 1.25 kU mL^{-1} or 2.5 kU mL^{-1}. The experiment was triplicated, and the average and standard deviation determined. After the gelation kinetics study, all other experiments were conducted at pH 6.5 as it appeared to be the optimal based on our experimental goals. To further validate our hypothesis, (that is the influence of iron(II) on the gelation kinetics) oscillatory time-sweep rheology was conducted to monitor the evolution of storage modulus (G') and loss modulus (G'') over time. The gelation point was determined as the crossover of G' and G''. Detailed rheological data is provided in the ESI† (Fig. S1 and S2).

2.3 Tyramine conversion to dopa by UV-visible spectroscopy

Tyramine from HATA conversion to dopa or the formation of iron–catechol complexes or conjugate products because of the crosslinking was monitored *via* UV-visible spectroscopy (Jasco V-750 spectrophotometer) according to methods already described elsewhere with modification.[13] The structural changes in HATA treated with either tyrosinase alone or a combination of tyrosinase and iron(II) were monitored over a thirty-minute time course at predetermined intervals. The spectra were acquired from 200–600 nm. Tyramine conversion to catechol and iron–catechol complexes were monitored at 320 nm whiles dimerization or coupling of quinones or catechol were monitored 570 nm. The final concentration of HATA, tyrosinase and iron(II) was 1.5 mg mL^{-1}, 0.650 kU mL^{-1} and 0.225 mM respectively. The reaction scheme is shown in Fig. 2.

2.4 Raman spectroscopy

Prior to Raman spectra acquisition, HATA was dissolved in acetate buffer (pH 6.5) for 3 hours at 60 °C and left to stir overnight at room temperature. Hydrogels were formed in a Teflon mould by mixing pre-dissolved tyrosinase or tyrosinase–iron(II) precursor solution in acetate buffer (pH 6.5) with HATA solution *via* two syringes connected by Combifix adaptor. The hydrogels were allowed to completely gel overnight in the fridge and lyophilized for the acquisition of Raman spectra. The Raman spectra were obtained using Raman spectroscope Renishaw inVia Qontor coupled with microscope Leica

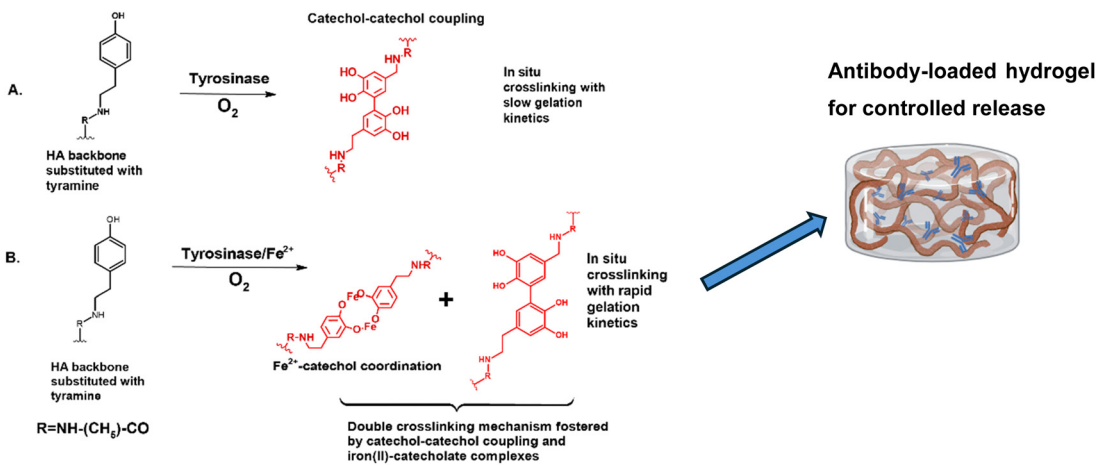

Fig. 1 Influence of iron(II) on hydrogel gelation kinetics (A) hydrogel formation catalysed by tyrosinase (B) rapid HATA hydrogel formation catalysed by iron(II) for the controlled release of antibodies.

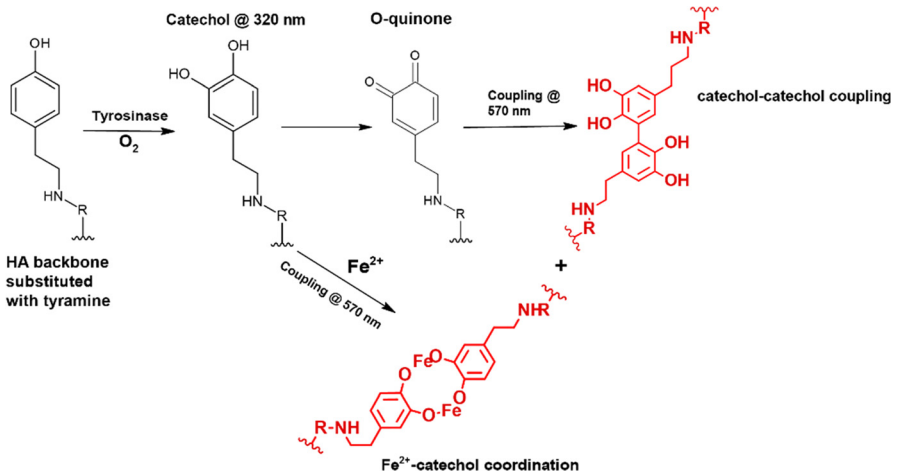

Fig. 2 Phenol conversion to catechol at 320 nm and resulting coupling products of iron(II)–catechol coordination and catechol–catechol coupling at 570 nm to form hydrogels.

DM2700M, software WiRE 5.1. The spectra were acquired under these conditions: objective of 100× PL, laser excitation of 633 nm, laser power of 10%, grating of 1800 l mm^{-1}, mapping step of 2 μm × 2 μm, exposure time of 1 s, accumulations of 100 and bleaching time of 120 s. Collected spectra were baseline subtracted (intelligent fitting), no normalisation was applied.

2.5 Hydrogels formation and viscoelastic properties

250 μL of precursor solutions of 2% w/v HATA dissolved in acetate buffer of pH 6.5 with 250 μL varying final concentrations of tyrosinase of 0.625 kU mL^{-1}, 1.25 kU mL^{-1}, and 2.5 kU mL^{-1} or its pre-dissolved counterpart with iron(II) in the concentration of 0.9 mM or 1.8 mM were used to form the hydrogels. The precursor solutions of the enzyme alone or enzyme pre-dissolved with iron(II) were homogenized with HATA *via* two syringes connected with a Combifix adaptor and quickly transferred into a Teflon mould with a diameter of 20 mm. The hydrogels were then left to completely solidify in the fridge overnight and its viscoelastic properties determined. The linear viscoelastic region was determined using an absolute rotational rheometer (Discovery HR-3 Rheometer TA Instruments) with an upper geometry of 20 mm. The measurement was performed at a constant frequency of 1 Hz, in the displacement range of 0.003–4 rad at 10 points per decade at 25 °C. Measurements were performed in triplicates and the average and standard deviation determined.

2.6 Hydrogels degradation test

Hydrogels stability under hyaluronidase was monitored as follows. Briefly, hydrogels were formed using rhodamine conjugated HATA which was synthesized by methods described elsewhere.[33] The hydrogels formation followed the same procedure already described here. The final concentration of tyrosinase in the hydrogel was 0.625 kU mL^{-1} with or without 0.9 mM or 1.8 mM iron(II) and 1% w/v HATA. The preformed hydrogel was fully immersed in the degradation media of 4.5 mL composed of 1 mg mL^{-1} bovine testes hyaluronidase and 0.2 mg mL^{-1} bovine serum albumin (BSA) in 0.05 M acetate buffer at a pH of 7. At predetermined time points, the whole media was aspirated and replaced with fresh media and the absorbance determined using UV-Visible spectrophotometer at 557 nm corresponding to the rhodamine's absorbance wavelength. Calibration curve based on HATA–rhodamine conjugate was established in the linear range of 6.25 to 400 μg mL^{-1} with a coefficient of correlation of 0.9996. The experiment was performed in triplicate and the average and standard deviation determined.

2.7 Cytotoxicity of hydrogels test

To evaluate the cytotoxicity of hydrogels, the 3-(4,5-dimethylthiazol-2-yl)-2,5-diphenyl-tetrazolium bromide (MTT) assay was performed with mouse fibroblastic cell line 3T3 cultivated in Dulbecco's Modified Eagle Medium supplemented with a 10% fetal bovine serum at 5% CO_2 atmosphere, 37 °C. The cells were seeded into 48-well plates at a concentration of 10 000 cells per well. After 24 hours, the culture medium was replaced with 500 μl of fresh medium, and 100 μl of hydrogels were preformed in sterile cell inserts with 0.4 μm pore polyethylene membrane. Subsequently, the cell inserts containing the hydrogels were immersed into the medium in the wells. The untreated controls received only 500 μl of fresh medium or 500 μl of fresh medium with empty cell inserts. After 48 h of incubation, the inserts were removed, and 50 μl of MTT (5 mg mL^{-1}) was added to each well. The plates were incubated for 2.5 h at 37 °C. Then the MTT solution was removed, 550 μl of a lysis solution (2-propanol, 10% dimethyl sulfoxide, 10% Triton X-100) was added, and lysis was carried out for 30 min at room temperature and 150 rpm. Finally, the absorbance of each well at 570 and 690 nm (A570 and A690, respectively) was read by an EnSight Multimode Plate Reader (PerkinElmer, Waltham, MA, USA). The obtained data were processed in Kaleido (PerkinElmer, Waltham, MA, USA). The final absorbance A was calculated as $A = A_{570} - A_{690}$. The change in the viability of the treated cells was calculated relative to the

negative control at 0 h ($A_{CTRL,0}$) according to eqn (1):

$$\text{Viability relative to control}(\%) = \frac{A}{A_{CTRL,0}} \quad (1)$$

2.8 Hydrogel loaded with human antibody (IgG) and release

Hydrogels containing Privigen® was produced by methods previously described in the hydrogel formation section. Briefly 100 mg mL^{-1} Privigen® was mixed homogeneously with 2% w/v HATA. The resulting solution was then mixed homogeneously with tyrosinase or tyrosinase pre-dissolved with iron(II). The final formulation consisting of 500 μL of hydrogel composed of 12.5 mg of Privigen® (IgG), 0.625 kU mL^{-1} with or without 0.9 mM iron(II) and 1% w/v HATA. This formulation combination of tyrosinase concentration and iron was chosen based on the cytotoxicity studies conducted. For the release studies, the hydrogels were fully immersed in 2 mL phosphate buffer saline (pH 7.4) and at predetermined time points, the whole medium was aspirated and replaced with fresh buffer solution. Protein concentration was determined in the release medium with the RC DC protein assay kit (Bio-Rad, Cat. No. 5000121) following the manufacturer's instructions. Absorbance was measured at 750 nm using a SpectraMax plate reader (Molecular Devices). The experiment was performed in triplicate and the average and standard deviation determined. The release curve was analysed using the Korsmeyer–Peppas mathematical model in eqn (2).

$$\frac{M_t}{M_\infty} = kt^n \quad (2)$$

where $\frac{M_t}{M_\infty}$ refers to the fraction of the drug released at time t, k is the release rate constant and n is the release exponent demonstrating the mechanism of drug release.[34]

2.9 Released antibody bioactivity

To validate the encapsulation and the release did not harm the bioactivity of the Fc-part of the antibody we performed western blot analysis and a Dot blot. For western blot analysis, an equal volume of solution was resolved by SDS-PAGE in 4–12% bis-Tris NuPAGE gel (10 wells) (Thermo Fisher Scientific). After migration, proteins were transferred to a nitrocellulose membrane using the Mini Trans-Blot Electrophoretic Transfer cell (Bio-Rad, Cat. No. 1703930). Transfer of proteins was validated using Ponceau-S. For Dot blot analysis, 2 μL of release solution were applied to a nitrocellulose membrane and let dried for 10 minutes. As a positive control Privigen® (1:100) and as negative control blank release solution was used. Unspecific binding was blocked by 5% BSA in TBS-T for 1 h at Room temperature under constant agitation. A peroxidase conjugated anti-human IgG (H + L) (Jackson Immunoresearch 109-035-003; RRID: AB_2337577) was diluted 1:30 000 in 5% BSA in TBS-T and incubated for 1 h at RT. The Licor WesternSure Premium chemiluminescence substrate (LiCor BioScience GmbH, Bad Homburg, Germany) was applied for chemiluminescence detection using the LiCor C-Digit blot scanner (LiCor).

2.10 Hydrogel swelling ratio

The swelling properties of hydrogels composed of HATA crosslinked with either tyrosinase or tyrosinase and iron(II) were assessed by fully submerging it in 9.5 mL of phosphate buffered saline pH 7.4 for 72 hours. The initial weight of the hydrogel before immersion was recorded as W_0. At specific time intervals, the hydrogels were taken out, and any excess water was carefully bloated using tissue paper. The experiment was performed in triplicate and the average and standard deviation determined. The new weight of the hydrogels was then recorded as W_1. The swelling ratio was calculated using eqn (3).

$$\text{Swelling ratio} = \frac{W_1 - W_0}{W_0} \times 100\% \quad (3)$$

2.11 Hydrogel mesh size and crosslinking density

The impact of iron(II) on hydrogel structure formation was assessed by calculating the molecular weight between crosslinks (M_c) using Peppas' method[35] and determining the mesh size (ξ) through rubber elasticity theory as proposed by Flory.[36] This theoretical framework explains how swelling behaviour relates to structural properties, with Mc influencing ξ, which represents the average spacing between cross-links in a swollen hydrogel.

The mesh size ξ was determined using eqn (4), derived from Flory's theory:

$$\xi = l v_{2,s}^{-\frac{1}{3}} \left(\frac{2C_n M_c}{M_r}\right)^{\frac{1}{2}} \quad (4)$$

In this eqn (l) denotes the virtual bond length, which corresponds to the distance between glycosidic oxygen atoms within a monosaccharide unit (0.52 nm for HATA[37]). C_n represents the Flory characteristic ratio (27 for HATA)[37] while M_r is the molar mass of the repeating disaccharide unit (400 g mol^{-1} for HA). Further details on the ξ calculation, including how ν_2,s and M_c were determined, can be found in the ESI.†

3.12 Test for mucoadhesion

Hydrogels crosslinked by tyrosinase (0.625 kU mL^{-1}) or its combination with iron(II) (0.625 kU mL^{-1}+ 0.9 mM Fe^{2+}) were evaluated for mucoadhesive properties. Briefly 20% w/v porcine gastric mucin type II dissolved in PBS (pH 6.5) was coated onto an adhesive tape applied on both lower and upper PU 20 geometries of rheometer (KinexusPro+ Malvern, United Kingdom). The measurement was done at 32 °C to mimic the physiological temperature of the nasal cavity.[38] A modified axial test for the determination of tack and adhesion predefined in the rSpace for Kinexus software was used. A circular hydrogel sample with a diameter of 20 mm was placed at the centre of the lower geometry. The gaping speed was set to 10 mm s^{-1}, the contact force was 0.25 N, and the contact time was 20 s. Adhesion was expressed as the maximum detachment force per contact area (mN mm^{-2}) and the measurements were performed in quadruplicate and averaged.

3 Results and discussion

3.1 Kinetics of gelation

Tyramine was conjugated to the hyaluronic acid backbone *via* a two-step reaction to make it viable for tyrosinase-induced crosslinking, followed by characterization using ^{1}H NMR for structural elucidation and determination of the degree of substitution of tyramine moieties (see ESI,† Fig. S4 for proton NMR spectra and Fig. S5 for the reaction scheme). The detailed synthetic procedure can be found in our publication.[30] SEC-MALLS was used for molecular weight determination as previously described.[30] A prerequisite for the development of *in situ* hydrogels for medical applications, such as intranasal administration, drug delivery, filling defective sites, or serving as blood-clotting agents, is that they have tuneable properties, such as fast gelation time and suitable mechanical strength, to prevent the possible leakage of therapeutic agents and address bleeding disorders.[27,39] Tyrosinase crosslinked hydrogels have been fabricated in the past for biomedical applications but have been characterized by poor mechanical properties and longer gelation times.[40] To overcome this challenge, we have produced *in situ* fast gellable hydrogels with suitable properties to render them fit for *in situ* nasal applications. In that vein, we have examined the effect of iron(II) on the kinetics of gelation of tyramine conjugated hyaluronic acid (HATA) hydrogels crosslinked by tyrosinase. The kinetics of gelation were monitored for both tyrosinase-modified hydrogels and iron(II)-catalysed tyrosinase hydrogels, where we probed various parameters such as enzyme concentration, pH, iron(II), and polymer concentration. We envisaged that our drug delivery system could potentially be applied in mucosal drug delivery, particularly for intranasal use; therefore, we selected pH levels of 5.6 and 6.5, which fall within the range of the nasal cavity's pH.[31] We observed that the hydrogel exhibited a significant dependence of gelation time on pH, enzyme, and polymer concentrations. Overall, longer gelation times were observed under varying polymer and enzyme concentrations or pH levels (Fig. 3(A)), consistent with previous reports.[27,40] At pH 5.6, we observed the longest gelation time ranging between 886 to 538 seconds dependent on polymer and enzyme concentration. Conversely, the benefits of higher polymer concentration and enzyme activity become more evident. The shortest gelation times were observed at the highest pH of 6.5 which also correlated positively with the enzyme concentration. (Fig. 3(A)).

Also, it has also been reported that tyrosinase is active from an acidic pH of 4.5 through to 9 where it loses about 60% of its catalytic activity with pH 6.5 being the optimal.[41] Also, under acidic conditions, protons are known to have inhibitory effect on the enzyme accounting for the high gelation times observed[42] (Fig. 3(A)) therefore slowing down the formation of

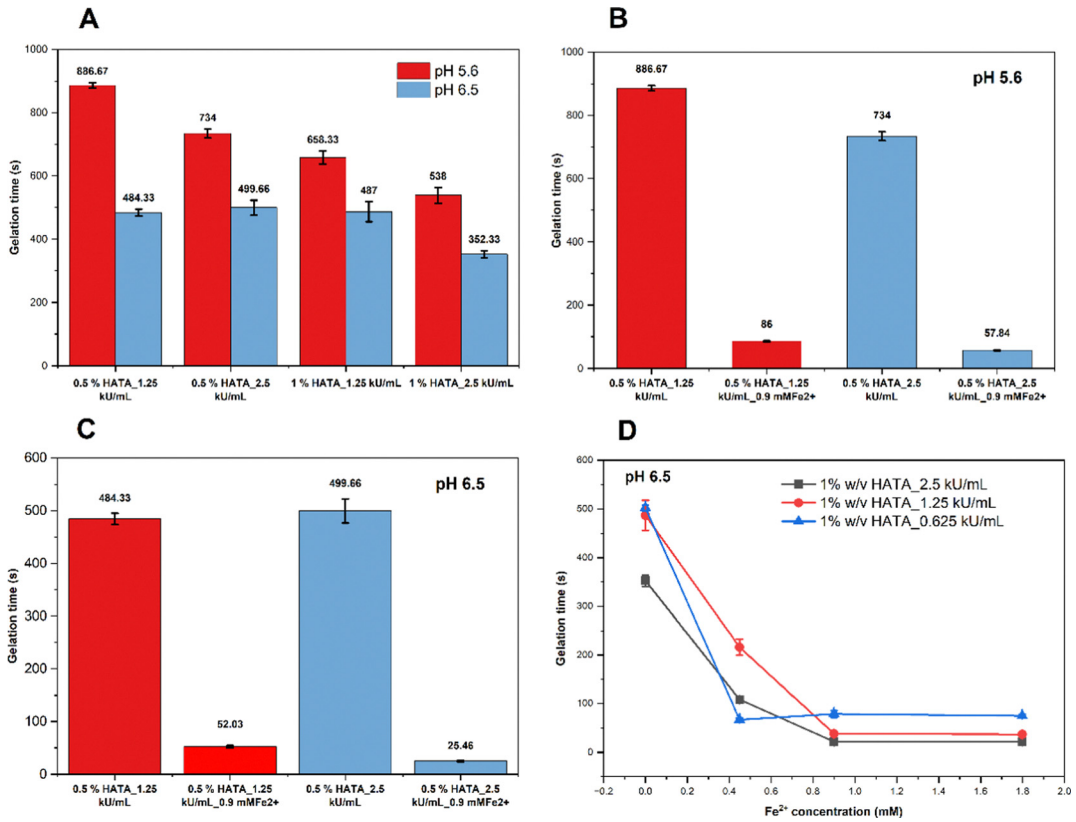

Fig. 3 Gelation kinetics determined *via* magnetic stirring as a function of pH, enzyme concentration, Fe^{2+} and polymer concentration. (A) Influence of pH, polymer concentration, and enzyme activity on gelation rate. (B) Influence of iron (II) on gelation kinetics at pH 5.6 (C) Influence of iron(II) on gelation kinetics at pH 6.5 (D) Influence of varying enzyme and iron concentration at pH 6.5 on gelation kinetics.

the polymer network. Overall, at a pH of 6.5, the crosslinking reaction occurs at a faster rate; however, the effects of increased polymer concentration and enzyme activity are less pronounced (Fig. 3(A)).

In Fig. 3(B) and (C), we assessed our hypothesis by probing the effect of catalytic amount of iron(II) on the kinetics of gelation of the hydrogels. The iron's presence resulted in rapid gel formation with more than ten folds decrease in the gelation time. We also observed similar trends with the effect of the pH. It was observed that at the acidic pH of 5.6, the gelation time significantly dropped from 86 seconds to approximately 58 seconds with increasing enzyme concentration and fixed iron(II) concentration (Fig. 3(B)). Similar trend was observed for the optimal pH of 6.5 where the gelation time of the enzyme was halved with increasing enzyme concentration (Fig. 3(C)). With the goal of developing safe biomaterials for biomedical applications, we further decreased the enzyme concentration while evaluating the effect of iron(II) on the gelation kinetics at a fixed pH of 6.5, keeping the polymer concentration constant (Fig. 3(D)). We observed that even at a low concentration of 0.625 kU mL^{-1} enzyme, the presence of iron(II) was able to decrease drastically the gelation time from about 500 seconds to 67 seconds where it plateaued irrespective of the iron (II) concentration (Fig. 3(D)). The gelation time, estimated visually, was further confirmed through rheological analysis, where the crossover of G' and G'' indicated the sol–gel transition. The corresponding rheological data is available in the ESI† (Fig. S1 and S2).

3.2 Tyramine conversion to catechol

The conversion of tyramine to catechol by tyrosinase leading to catechol–catechol dimerization in the presence of molecular oxygen was monitored by UV-VIS spectrophotometry. Further, iron(II)–catechol coordination complex formation by iron(II)-catalysed tyrosinase was also monitored *via* UV-VIS spectrophotometry according to the scheme described in Fig. 2. During the formation of tyrosinase crosslinked hydrogel, phenolic groups are converted from monophenol to orthodiphenols or orthoquinones. From our results obtained, the formation of dopa or catechol can be monitored at 280 or 325 nm (Fig. 4(A)) but due to the unavoidable interference from other aromatic groups such as tyramine which also absorbs at 280 nm (see ESI,† Fig. S3 for UV-visible spectra of DOPA standard), the reaction was monitored at 320 nm which has higher molar absorptivity compared to 280 nm. Dopa or catechol formation has been monitored at 310 nm[43] nm and 350 nm[13] in previous studies.

In general, there was a time dependent increase in the rate of catechol formation in both tyrosinase and iron(II)-catalysed tyrosinase hydrogels evidenced by the increase in absorbance (Fig. 4(A) and (B)). However, the rate of catechol conversion was about two times faster in the presence of iron(II) compared to the enzyme alone (Fig. 4(C)) with a time dependent increase in the conversion rate.

As a copper containing enzyme, the mechanism by which iron(II) catalysis tyrosinase lies in its ability to eliminate the hysteresis associated with the interconversion between the four discrete states during its monooxygenase or oxidative catalytic activity.[28] It does so through the reduction of Cu^{2+} at the active site of the enzyme.[28] From Fig. 4(B), we also observed a disappearance of the maxima at 320 nm where we postulated the possible formation of iron–catecholate complexes associated with the Fenton's reaction already reported.[44,45] Surprisingly, we observed a maximum at 570 nm (Fig. 4(A) and (B)) for both tyrosinase and iron(II)–tyrosinase treated hydrogels which was not reported in the previous work where tyrosine conversion to dopa by tyrosinase was studied.[13] Owing to this, we propose two possible crosslinking mechanisms: the dimerization of catechol groups and the formation of iron–catechol bis species, as described in the reaction scheme in Fig. 2. The formation of iron–catechol bis species occurs within a pH range of 6–7, which aligns with our experimental pH of 6.5, as demonstrated by previous studies.[46] This dual crosslinking mechanism is expected to enhance the mechanical properties of the hydrogels. Due to the presence of iron(II), the conversion rate was about two times higher dependent on time in comparison to its counterpart (Fig. 4(D)).

3.3 Raman spectroscopy

To better understand the iron(II)-catalysed tyrosinase hydrogels (HATA_TYR_Fe^{2+}) and the formation of the iron–catecholate complex, Raman spectra of the standard compounds $FeSO_4 \cdot 7H_2O$ and HATA_TYR (tyrosinase-crosslinked) hydrogels were also measured. Raman spectra in the region from 100 cm^{-1} to 1275 cm^{-1} are shown in Fig. 5(A), while those from 950 cm^{-1} to 2000 cm^{-1} are shown in Fig. 5(B). A zoomed-in region from 100 cm^{-1} to 1000 cm^{-1} is presented in Fig. 5(C). Focusing on the spectrum of the HATA_TYR_Fe^{2+} sample (Fig. 5(C)), Raman shifts at 120 cm^{-1}, 150 cm^{-1}, and 470–480 cm^{-1} correspond to lattice vibrations and confirm the presence of iron(II) in HATA_TYR_Fe^{2+}. In the same region, vibrations associated with C–H groups and C–C bonds of phenol are also observed. Shifts in Raman peaks to the left or right indicate an interaction between $FeSO_4 \cdot 7H_2O$ and HATA_TYR. This interaction is further evidenced by changes in peak intensity along the *y*-axis.[47] The bands at 620 cm^{-1} and 650 cm^{-1} indicate an interaction between iron(II) and the phenolic oxygen of catechol, as shown in Fig. 5(C).[45,48] The mentioned interaction is illustrated in the reaction scheme in Fig. 1(B). The most intense band at 930 cm^{-1} corresponds to C–C and C–O–C bonds, which are part of the hyaluronic acid structure. The peak around 975 cm^{-1} (Fig. 5(A)-i) is attributed to SO_4^{2-} ($FeSO_4 \cdot 7H_2O$).

The presence of HATA_TYR in HATA_TYR_Fe^{2+} is more clearly recognizable in the Fig. 5Bii spectrum. The band at 1060 cm^{-1} corresponds to C–O and C–C bonds, while the band at 1125 cm^{-1} represents C–H and C–OH bonds. The peak at 1295 cm^{-1} is associated with CH_2, and bands corresponding to C–H, C–N, and CH_2 are observed in the range of 1400 cm^{-1} to 1460 cm^{-1}.[49] It can be observed that there are no responses at 1600 cm^{-1} and 1760 cm^{-1} in the sample spectrum. This may suggest a specific spatial arrangement of the HATA_TYR_Fe^{2+} structure, where the hyaluronic acid backbone is positioned

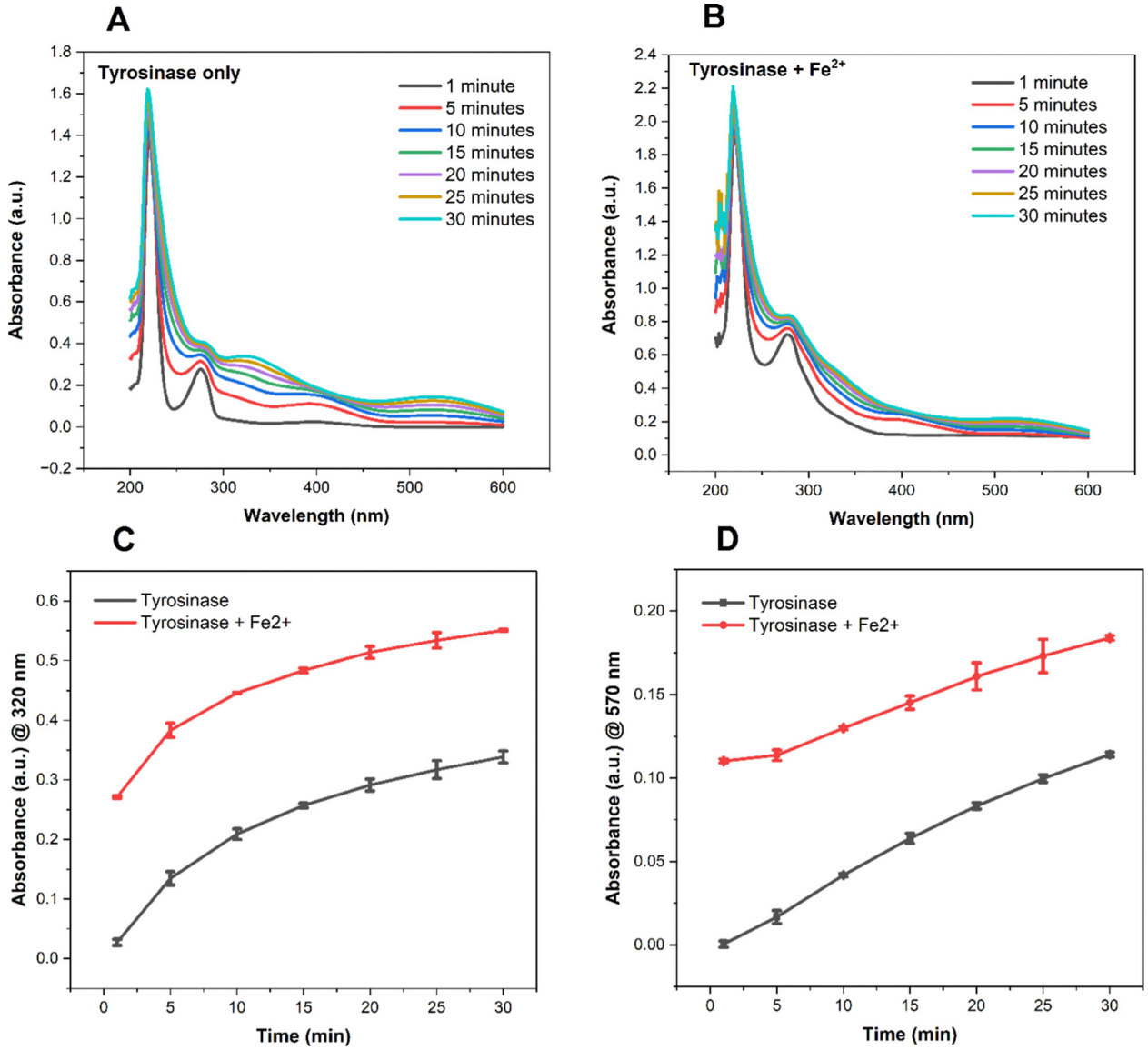

Fig. 4 UV/VIS spectroscopy evaluation of catechol and its product formation from tyramine conjugated HA (HATA) catalysed by tyrosinase or iron(II) tyrosinase crosslinking. (A) Tyrosinase only crosslinked hydrogels (B) tyrosinase + iron (II) (C) comparison of conversion rate between tyrosinase catalysed or its combination with iron(II) monitored at 320 nm (D) rate of the formation of conjugation products of catechol–catechol dimerization or iron–catecholate complexes formation monitored at 570 nm.

externally to the Fe^{2+}–catechol part of the complex.[48] That is why the responses of the benzene ring in HATA_TYR_Fe^{2+} appear within the noise. As evidenced by Raman measurements and UV/Vis results, Fe^{2+} was successfully incorporated into the HATA_TYR structure.

3.4 Viscoelastic properties of hydrogels

Hydrogels are subjected to various mechanical stresses in biomedical applications, such as drug delivery, wound dressings, and medical implants, just to name a few.[50] Therefore, the need to evaluate their rheological properties. The viscoelastic properties of the hydrogels were analysed in oscillation mode where the effect of iron(II) at two different concentrations, tyrosinase concentration and a fixed polymer concentration were evaluated.

All the hydrogels exhibited the dominance of the elastic properties with $\tan\delta$ values < 0.1 in the linear viscoelastic region examined. First, at varying enzyme concentrations, the final G' values of the hydrogels were comparable, and no effect of increased enzyme activity was observed. Secondly, the presence of iron(II) leads to an increase in the final G' values, independent of enzyme concentration (Fig. 6). The impact of iron(II) is evident across all formulations, as it reinforces crosslinks between polymer chains, leading to an increase in storage modulus. This observation further supports our proposed double crosslinking mechanism mentioned in Section 3.2, where catechol–catechol dimerization and iron(II)–catechol complex formation occur through the Fenton reaction, as previously reported.[44,51]

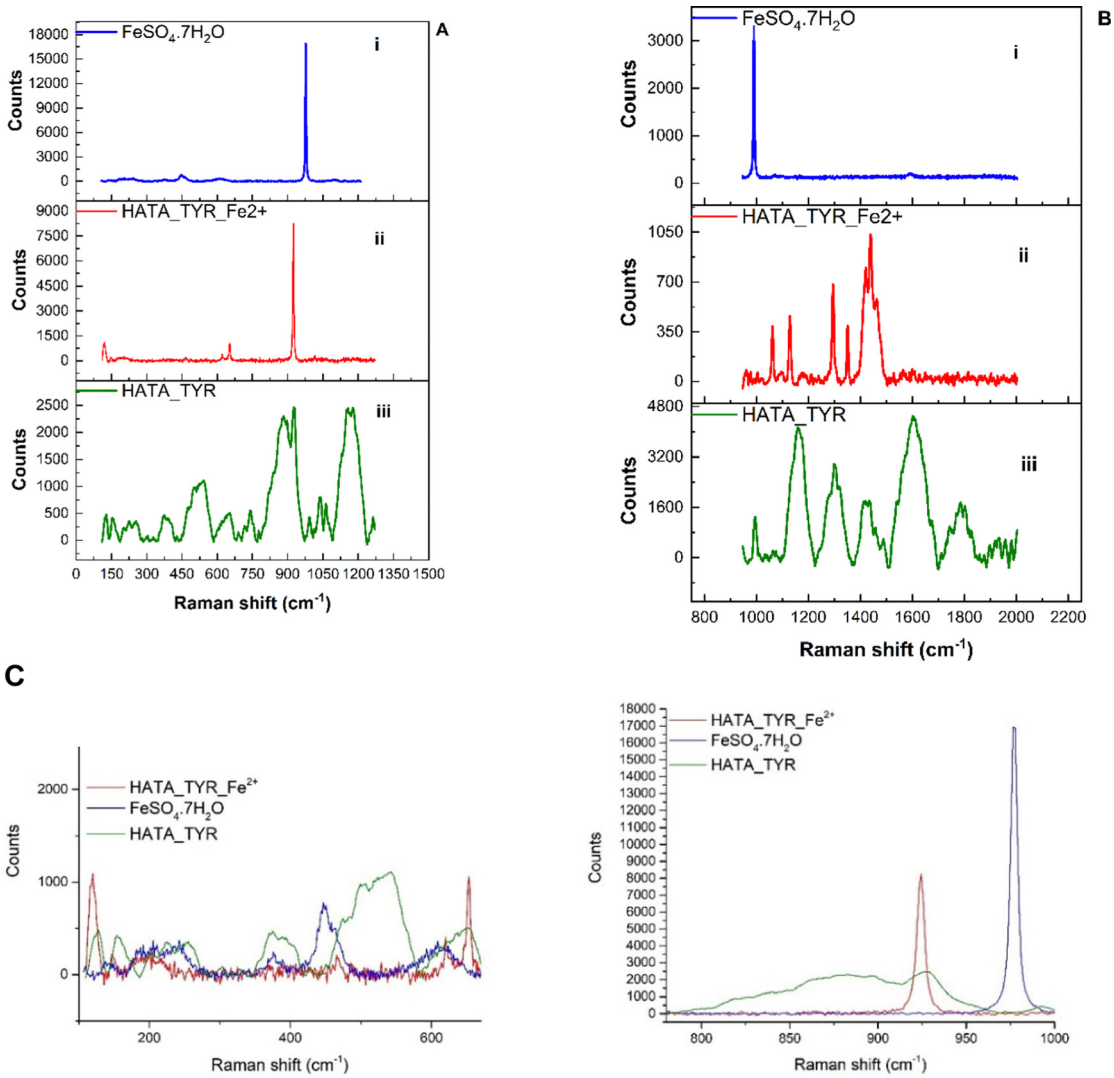

Fig. 5 Raman spectra of $FeSO_4{\cdot}7H_2O$ (i), HATA_TYR (iii) and sample HATA_TYR_Fe^{2+} (ii) in spectral regions from 100 cm^{-1} to 1275 cm^{-1} (A) and from 950 cm^{-1} to 2000 cm^{-1} (B). Zoomed in Raman spectra of $FeSO_4{\cdot}7H_2O$, HATA_TYR and sample HATA_TYR_Fe^{2+} in spectral region from 100 cm^{-1} to 1000 cm^{-1} (C).

3.5 Hydrogel cytotoxicity

The cytotoxicity of hydrogels crosslinked with varying concentrations of enzymes (2.5 kU mL^{-1}, 1.25 kU mL^{-1} and 0.625 kU mL^{-1}) in the presence or absence of iron(II) at fixed 1% HATA was evaluated *via* MTT assay. There was a dose dependent cytotoxicity of the tyrosinase on the cells with higher concentrations of the enzyme being weakly cytotoxic inhibiting about 40% of the cell growth (Fig. 7(A)).

As demonstrated in Fig. 7(B), the effect of iron(II) on the cytotoxicity of the hydrogels was more evident at the lower enzyme concentration of 0.625 kU mL^{-1}. It is worth noting that the crosslinking of tyrosinase hydrogels requires molecular oxygen to proceed; therefore, the cells could have been oxygen-deprived as they had to compete for oxygen during the curing of the hydrogels.[22] This phenomenon, where cells are deprived of oxygen and ultimately die, is known as hypoxia.[52] It is being mitigated by carefully optimizing the iron(II) and tyrosinase concentration as demonstrated in our work (Fig. 7(B)). Although we did not directly confirm that oxygen consumption during the crosslinking reaction induced hypoxia, previous studies have reported that the hypoxic activity of tyrosinase is analogous to that of glucose oxidase hydrogels, which consume oxygen during curing to create a hypoxic environment.[53] Following the cytotoxicity studies, 0.625 kU mL^{-1} or 0.625 kU mL^{-1} with 0.9 mM of iron(II) was chosen for further experiments.

3.6 Hydrogel swelling

The swelling properties of hydrogels are important, as they play a vital role in how drugs are released from the hydrogel matrix to their site of action. The polymers used in formulating hydrogels can absorb large amounts of water, creating a sponge-like structure that allows the diffusion of therapeutic agents. It is therefore essential to tailor the swelling properties of hydrogels based on the goals of the drug delivery system being designed.[54]

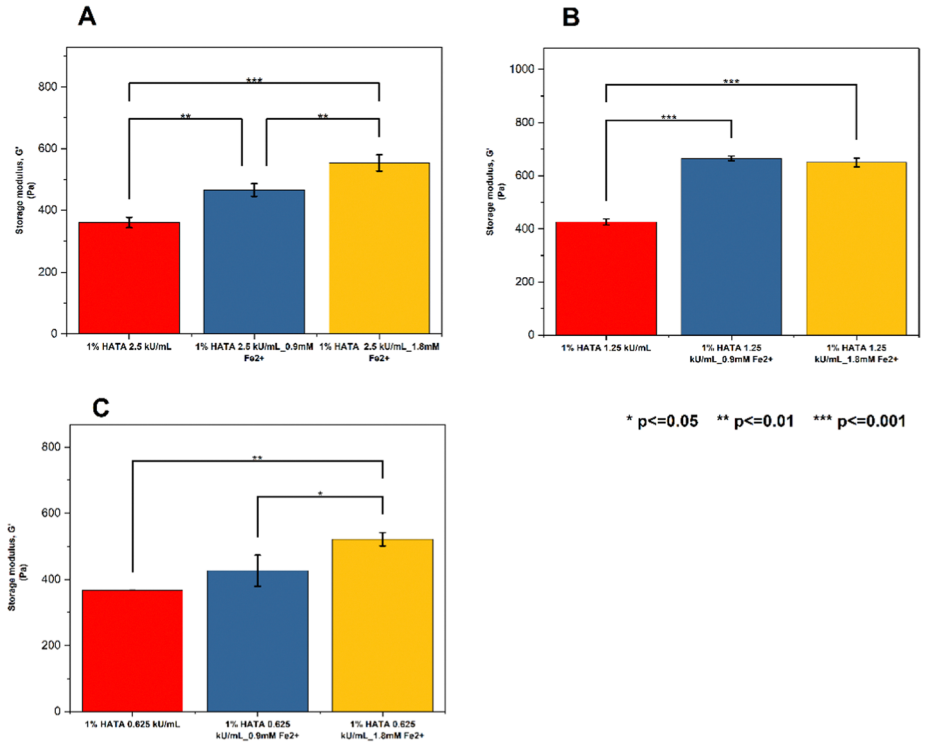

Fig. 6 Rheological measurements of the viscoelastic properties of hydrogels at iron (II) concentrations of 0.9 mM or 1.8 mM. (A) G' at 2.5 kU mL^{-1} (B) G' at 1.25 kU mL^{-1} (C) G' at 0.625 kU mL^{-1}.

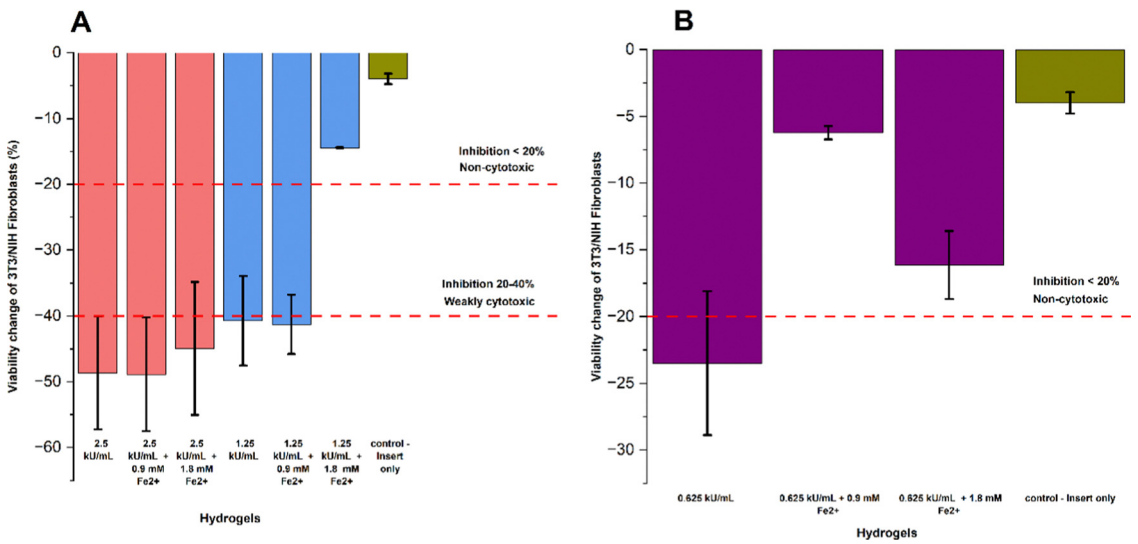

Fig. 7 Cytotoxicity of hydrogels on 3T3/NIH fibroblasts evaluated using the MTT assay. (A) Cytotoxicity levels based on iron(II) concentrations of 0.9 or 1.8 mM and the corresponding tyrosinase concentration of 1.25 or 2.5 kU mL^{-1} and insert used as control. (B) Cytotoxicity levels of the lowest enzyme concentration tested at 0.625 kU mL^{-1} and the corresponding iron(II) concentrations of 0.9 or 1.8 mM and insert used as control.

In Fig. 8 we evaluated the swelling properties of hydrogels crosslinked by tyrosinase or iron(II)–tyrosinase. From our results, it is evident that the presence of iron(II) significantly affects the swelling properties of hydrogels especially in the first few hours (swelling ratio of 5% for tyrosinase only crosslinked hydrogels *versus* 1% of their iron(II)-catalysed counterparts) owing to the formation of additional crosslinks alongside catechol–catechol dimerization. Iron(II) hydrogels are known to have enhanced mechanical properties which further impedes the hydrogels water absorption.[55] It is demonstrated by swelling ratio slightly above 0% (Fig. 8). In the first few hours, both hydrogels transitioned from non-swelling state to shrinkable state as their swelling ratios fell below zero.[54] These types of hydrogels could potentially be employed as drug delivery

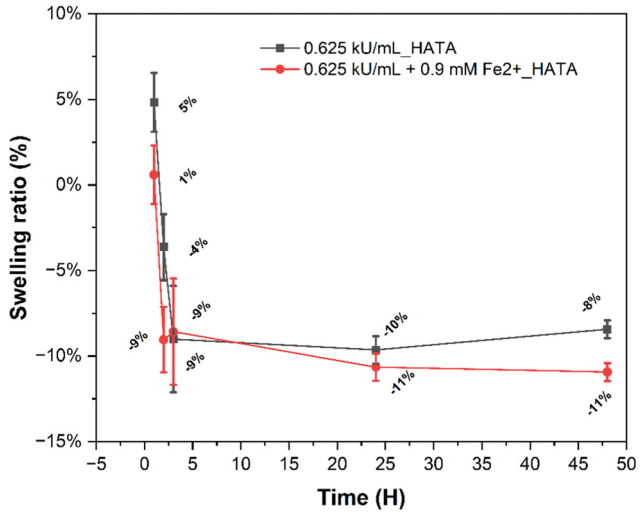

Fig. 8 Swelling behaviour of hydrogels over time.

systems and be used as adhesives as they are stable under physiological conditions. In their shrinkable state (<0% swelling ratio), they can also be used as dynamic stiffening and contraction agents and promote cell attachment and condensation.[56,57]

3.7 Antibody release

Two formulations containing 1% HATA crosslinked with tyrosinase (0.625 kU mL^{-1}) or its combination with iron(II) (0.9 mM) were loaded with Privigen® for an *in vitro* dissolution assay.

The released antibody concentration was evaluated by protein assay kit available commercially following the manufacturer's guide and the results shown in Fig. 9. In the first eight hours we observed a burst release of the antibodies of 61% (Tyr_ctrl) and 53% (Tyr_Fe^{2+}) which is quite high. This burst release could be associated with the initial swelling of the hydrogels in the first few hours as demonstrated by the swelling

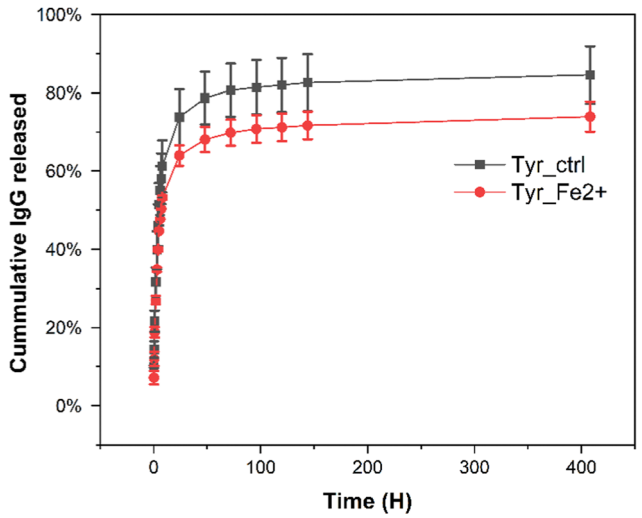

Fig. 9 Release of Privigen® from hydrogels. Tyr_ctrl (0.625 kU mL^{-1}) and Tyr_Fe^{2+} (0.625 kU mL^{-1} + 0.9 mM Fe^{2+}).

experiments in Fig. 8, which leads to the rapid diffusion of surface-adsorbed or weakly bound antibodies.[58] However, this observation is not surprising, considering that the hydrogels contain 1% w/v of the structural polymer. Therefore, it is expected that the hydrogels swell rapidly and release the antibody quickly in the first few hours. Nevertheless, the presence of iron(II) significantly slowed down the burst effect. Additionally, iron(II) in the formulation influenced the T50, the time required for 50% of the antibody to be released from the hydrogel.[59] Tyrosinase crosslinked hydrogel had a T50 of 5 hours whiles its combination with iron (II) increased the T50 by 2 hours. This observation agrees with our already validated hypothesis that the presence of the iron(II) further increases the crosslinking density of the hydrogels consequently affecting the release rate of the antibody. The experiment also demonstrates that the hydrogel can release the antibody. The rate of release will be affected by the surrounding environment, for instance, the release will be much slower on the surface of the nasal mucosa. The release curves were mathematically modelled using the Korse–Meyer Peppas equation described in eqn (1) and the results shown in Table 1. From the model fitting, release of antibodies from both formulations is Fickian diffusion driven with n values below 0.5 with a slight increase in release rate constant, k of the iron(II) tyrosinase crosslinked hydrogels with respect to the control sample (Table 1). In the first 8 hours, tyrosinase crosslinked hydrogels released 61% of the loaded antibody whiles the iron(II) tyrosinase crosslinked counterpart released 53% followed by sustained release for two weeks. The sustained release by the hydrogels can also be associated with the low swelling nature of the hydrogels which controls the rate of diffusion of therapeutic agents.[6] At the end of the study, tyrosinase crosslinked formulation released 85% of the total antibody loaded whiles the iron(II) tyrosinase crosslinked hydrogels released 74%. Iron(II)'s influence on the total released antibodies stems from the additional crosslinking density it imparts to the hydrogels, making the crosslinked network more tightly packed compared to the tyrosinase-catalysed hydrogels eventually affecting the total amount of antibodies released.

3.8 Hydrogel mesh size (ξ), crosslinking density, and molecular weight between crosslinks (M_c)

The mesh size of a hydrogel refers to the average distance between two adjacent crosslinks in a hydrogel network.[60] It also defines the space available within the hydrogel structure for molecular diffusion, making it a critical parameter in applications like drug delivery, tissue engineering, and filtration.[61] The M_c, designated as the average molecular weight between crosslinks, represents the spacing and density of cross-links, which

Table 1 Korse–Meyer Peppas fitting model parameters

Hydrogels	k	n	R^2
Tyr_ctrl	0.3452	0.1804	0.9189
Tyr_Fe^{2+}	0.2970	0.1825	0.9183

also influences the hydrogel's swelling capacity. Therefore, ξ and M_c are inversely related to cross-linking density an increase in cross-linking density leads to a decrease in ξ and M_c, which in turn affects the release of therapeutic agents.

Our results from the two formulations described in the release studies (see ESI† for detailed calculations) show a mesh size of 528 nm for tyrosinase hydrogels and 555 nm for iron(II)-catalysed tyrosinase hydrogels, with no significant difference ($p > 0.05$). Considering that human IgG, with a molecular weight of 150 kDa, has a hydrodynamic radius of 5.29 nm,[62] it was not surprising to observe a burst effect in both hydrogels during the first 8 hours of the release study. Also, given that the two formulations selected for release studies had comparable viscoelastic properties (Fig. 6(C)), it was not surprising to have observed comparable mesh size, crosslinking density and average molecular weight between the crosslinks. The cross-linking density was reported as 4.04 g m^{-3} for tyrosinase-crosslinked hydrogels and 3.92 g m^{-3} for their iron(II)-catalysed counterparts. The average molecular weight between cross-links was determined to be 321 kDa for tyrosinase hydrogels and 331 kDa for iron(II)-catalysed hydrogels, with no statistically significant differences. Based on these findings, it was concluded that the presence of iron(II) had minimal influence on mesh size, cross-linking density, and the average molecular weight between cross-links of the hydrogels. This highlights a range of factors that could contribute to antibody diffusion from the hydrogels, such as the pH, the ionic strength of the surrounding environment, hydrogel swelling, the degradation rate of the hydrogel matrix, and potential interactions between the hydrogel network and the antibodies.

3.9 Released antibody bioactivity

To validate that the tyrosinase or its combination with iron(II) cross-linking reaction did not affect the antibody bioactivity we performed Western and dot blot analysis. First, reduced and denaturated proteins within the releasing solution were separated electrophoretically. Ponceau-S staining showed two distinct bands at 50 kDa and 25 kDa for all samples examined. Those bands indicate intact heavy and light chains of the antibody and might suggest no cross-reaction amongst proteins, because of missing bands at various molecular weights (Fig. 10(A)). In addition, we performed dot blot analysis on native unreduced antibodies to validate that potential tyrosinase or its combination with iron(II) reaction products did not interfere with the bioactivity of the antibody. The data suggest that the tyrosinase reaction did not affect the antibody. It even indirectly indicates no effect on the bioactivity of the antibody (Fig. 10(B)).

3.10 Hydrogels degradation

Hyaluronic acid degradation test is indispensable especially in ascertaining its safety in various biomedical applications.[63] In the development of drug delivery systems, it directly impacts the rate at which therapeutic agents are released from the formulations.[64] In our study, we have evaluated the impact of the iron(II) on the degradation rate of the hydrogels owing to the additional crosslinking density imparted onto them. We observed that in the absence of the iron(II) (1% HATA_tyr) about 60% of the hydrogels was degraded in the presence of bovine hyaluronidase with respect to about 40% in the iron(II) loaded counterparts halfway through the experiment (Fig. 11). The differences in iron(II) concentration did not affect degradation rate of the hydrogels as we did not observe any significant differences.

At the end of the eight hours, only 70% of the iron(II) containing hydrogels was degraded in comparison to 100% of the control (Fig. 11).

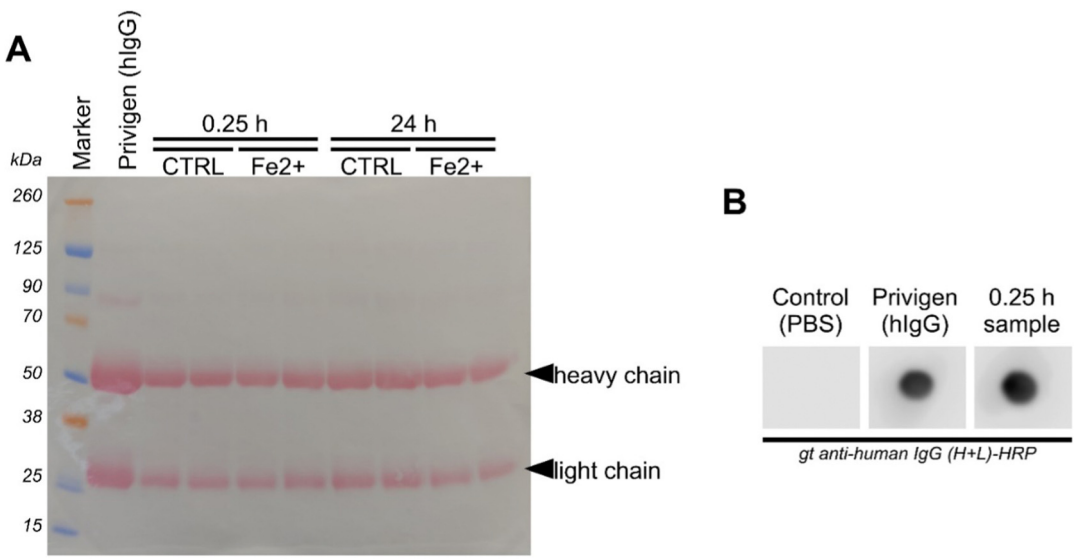

Fig. 10 Antibody bioactivity tests: (A) reduced western blot detection of proteins in the released medium by Ponceau-S protein detection. As a positive control, Privigen was used. The band at 50 kDa indicate the heavy chain and the band at 25 kDa the light chain of the antibody. (B) Dot blot detection of non-reduced human antibodies by chemoluminescence detection. As a positive control, Privigen was used. As a negative control, PBS was used and compared to a sample of the release study (0.25 h).

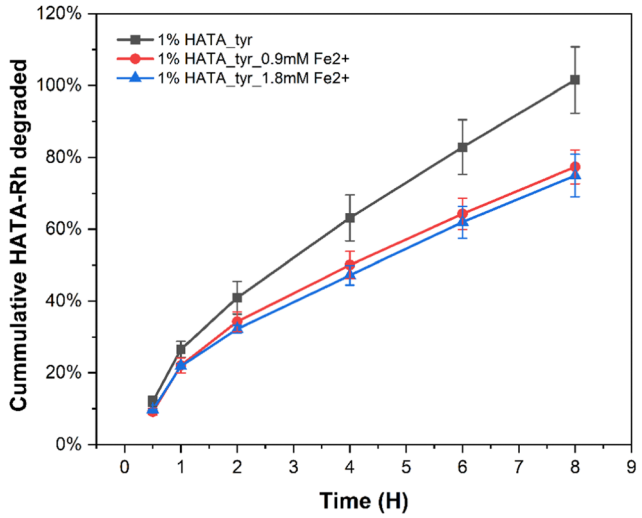

Fig. 11 Hydrogel degradation study conducted at two different iron(II) concentrations (0.9 mM or 1.8 mM) with a fixed polymer concentration (1% HATA) and enzyme concentration (0.625 kU mL^{-1}) at pH 6.5 in the presence of hyaluronidase.

3.11 Mucoadhesion of hydrogels

Tyrosinase crosslinked hydrogels are known to possess exceptional mucoadhesive properties owing to its ability to establish covalent bonds with thiols, hydroxyls or amine containing groups in mucins following its reactive oxidation products.[27] Also, the aromatic products formed from tyrosinase oxidized hydrogels can enhance the interaction between the hydrophobic regions of the mucin glycoproteins further enhancing the mucoadhesive properties of our nasal formulation.[14] Following an optimized formulation, the mucoadhesive properties of the hydrogels were tested. The presence of iron(II) significantly affected the mucoadhesive properties of the hydrogels as evidenced by the slight increase in mucoadhesive properties (Fig. 12). While this may appear to be surprising given that the viscoelastic properties (Fig. 6(C)) of these two formulations did not show any notable differences we weren't expecting this differences in mucoadhesive properties. This assumption is based on the relationship between mucoadhesive properties of hydrogels and their viscoelastic properties.[65]

However, given the complex nature of mucoadhesion as a phenomenon, the presence of the iron(II) might have enhanced the mucoadhesive properties through the metallic bonding between amino acids in mucin glycoproteins such as aspartic acid as previously described computationally.[66]

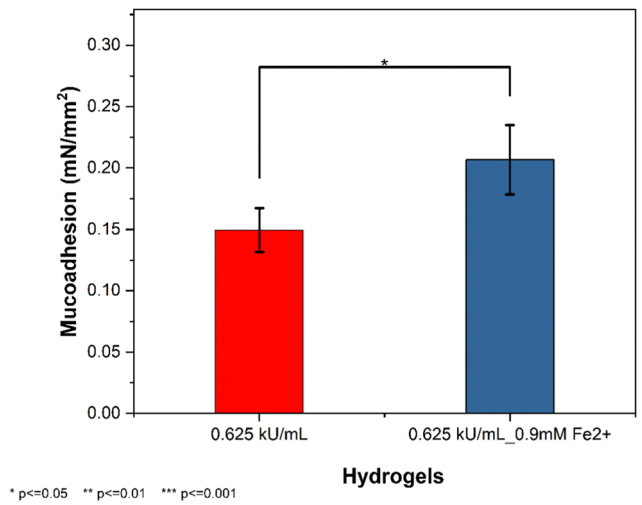

Fig. 12 Mucoadhesive properties of hydrogels determined using a rotational rheometer in the presence or absence of Fe^{2+} at a fixed HATA concentration (1% w/v).

4 Conclusion

In our study, we have formulated fast *in situ* iron(II) catalysed tyrosinase hydrogels potentially applicable for intranasal drug delivery. This fast *in situ* gellable hydrogels was previously impossible to produce except through high enzyme concentration, tyrosinase combination with other enzymes, or the use of tyrosinase recombinant form with its associated challenges. The incorporation of iron(II) significantly decreased the gelation time by an order of a magnitude even at significantly low enzyme concentration. These new hydrogels have the capacity to encapsulate and release antibodies in a controlled manner for two weeks without its crosslinking chemistry affecting the bioactivity of the antibodies. The hydrogels also have improved rheological properties thanks to the presence of iron(II) which eventually biodegrades in the presence of hyaluronidase. The hydrogels are biocompatible, making them safe for their intended use. Also, the presence of iron(II) enhances the hydrogels mucoadhesive properties to some extent. We envisage that these new hydrogels could find potential applications in the broader field of drug delivery particularly to mucus-rich surfaces.

Data availability

Data for this article, including UV-vis spectrophotometry for tyramine conversion to DOPA, Raman spectroscopy, gel blot and dot blot are available at Open Science Framework at URL **https://osf.io/8j2ye** with DOI 10.17605/OSF.IO/6YV8J.

Conflicts of interest

Vladimír Velebný has a financial interest in Contipro a.s., Dolní Dobrouč, Czech Republic, a commercial producer of hyaluronic acid. Martin Pravda, Jana Matonohová and Tereza Bártová are employees of Contipro a.s.

Acknowledgements

This project has received funding from the European Union's Horizon 2020 research and innovation programme under the Marie Skłodowska-Curie grant agreement No. 956977, and from the Ministry of Education, Youth and Sports of the Czech

Republic (MEYS CZ) under grant agreement No. SVV 260661 and the Cooperation Program (research area: PharmSci).

References

1 H. M. Shepard, G. L. Phillips, C. D. Thanos and M. Feldmann, *Clin. Med.*, 2017, **17**, 220.
2 S. Crescioli, H. Kaplon, A. Chenoweth, L. Wang, J. Visweswaraiah and J. M. Reichert, *MAbs*, 2024, **16**, 1–36, DOI: **10.1080/19420862.2023.2297450**.
3 N. A. Fletcher, L. R. Babcock, E. A. Murray and M. D. Krebs, *Mater. Sci. Eng., C*, 2016, **59**, 801–806.
4 G. P. Adams and L. M. Weiner, *Nat. Biotechnol.*, 2005, **23**, 1147–1157, DOI: **10.1038/nbt1137**.
5 M. R. Gilbert, J. J. Dignam, T. S. Armstrong, J. S. Wefel, D. T. Blumenthal, M. A. Vogelbaum, H. Colman, A. Chakravarti, S. Pugh, M. Won, R. Jeraj, P. D. Brown, K. A. Jaeckle, D. Schiff, V. W. Stieber, D. G. Brachman, M. Werner-Wasik, I. W. Tremont-Lukats, E. P. Sulman, K. D. Aldape, W. J. Curran Jr. and M. P. Mehta, *N. Engl. J. Med.*, 2014, **370**, 699–708.
6 R. Egbu, S. Brocchini, P. T. Khaw and S. Awwad, *Eur. J. Pharm. Biopharm.*, 2018, **124**, 95–103.
7 J. M. Schieferstein, P. Reichert, C. N. Narasimhan, X. Yang and P. S. Doyle, *Adv. Ther.*, 2021, 1–8, DOI: **10.1002/adtp.202000216**.
8 W. M. Tian, C. L. Zhang, S. P. Hou, X. Yu, F. Z. Cui, Q. Y. Xu, S. L. Sheng, H. Cui and H. D. Li, *J. Controlled Release*, 2005, **102**, 13–22.
9 S. Salehi-Had and W. M. Saltzman, Controlled intracranial delivery of antibodies in the rat, in *Protein Formulation and Delivery*, ed. J. L. Cleland and R. Langer, ACS Symposium Series, 1994, vol. 567, pp. 278–291.
10 Y. T. Wei, Y. He, C. L. Xu, Y. Wang, B. F. Liu, X. M. Wang, X. D. Sun, F. Z. Cui and Q. Y. Xu, *J. Biomed. Mater. Res., Part B*, 2010, **95**, 110–117.
11 J. C. Stanwick, M. D. Baumann and M. S. Shoichet, *Int. J. Pharm.*, 2012, **426**, 284–290.
12 S. H. Kim, S. H. Lee, J. E. Lee, S. J. Park, K. Kim, I. S. Kim, Y. S. Lee, N. S. Hwang and B. G. Kim, *Biomaterials*, 2018, **178**, 401–412.
13 Y. Chan Choi, J. S. Choi, Y. J. Jung and Y. W. Cho, *J. Mater. Chem. B*, 2014, **2**, 201–209.
14 S. Choi, H. Ahn and S. H. Kim, *J. Appl. Polym. Sci.*, 2022, **139**, 1–22, DOI: **10.1002/app.51887**.
15 W. Song, J. Ko, Y. H. Choi and N. S. Hwang, *APL Bioeng*, 2021, **5**, 1–22, DOI: **10.1063/5.0037793**.
16 R. Naranjo-Alcazar, S. Bendix, T. Groth and G. Gallego Ferrer, *Gels*, 2023, **9**, 230.
17 M. Nam, J. W. Lee and G. D. Cha, *Gels*, 2024, **10**, 640.
18 T. Chen, H. D. Embree, E. M. Brown, M. M. Taylor and G. F. Payne, *Biomaterials*, 2003, **24**, 2831–2841.
19 R. M. A. Maddock, G. J. Pollard, N. G. Moreau, J. J. Perry and P. R. Race, *Biopolymers*, 2020, **111**, e23390.
20 S. H. Kim, K. Kim, B. S. Kim, Y. H. An, U. J. Lee, S. H. Lee, S. L. Kim, B. G. Kim and N. S. Hwang, *Biomaterials*, 2020, **242**, DOI: **10.1016/j.biomaterials.2020.119905**.
21 H. Lee, N. F. Scherer and P. B. Messersmith, *Proc. Natl. Acad. Sci. U. S. A.*, 2006, **103**, 12999–13003.
22 S. Choi, H. Ahn and S. H. Kim, *J. Appl. Polym. Sci.*, 2022, **139**, 51887.
23 G. D. Degen, C. A. Stevens, G. Cárcamo-Oyarce, J. Song, R. Bej, P. Tang, K. Ribbeck, R. Haag and G. H. McKinley, *Proc. Natl. Acad. Sci. U. S. A.*, 2025, **122**, e2415927122.
24 J. Cabanes, F. García-Carmona, F. García-Cánovas, J. L. Iborra and J. A. Lozano, *Biochim. Biophys. Acta, Protein Struct. Mol. Enzymol.*, 1984, **790**, 101–107.
25 U. C. Galgatte, A. B. Kumbhar and P. D. Chaudhari, *Drug Delivery*, 2014, **21**, 62–73.
26 N. Ivanova, N. Ermenlieva, L. Simeonova, N. Vilhelmova-Ilieva, K. Bratoeva, G. Stoyanov and V. Andonova, *Gels*, 2024, **10**, DOI: **10.3390/gels10060385**.
27 P. Le Thi, Y. Lee, D. H. Nguyen and K. D. Park, *J. Mater. Chem. B*, 2017, **5**, 757–764.
28 A. Palumbo, G. Misuraca and G. Prota, *Biochem. J.*, 1985, **228**, 647–651.
29 C. A. Chrvala and A. Caspi, The product profiler, 2011.
30 E. Toropitsyn, M. Pravda, D. Rebenda, I. Ščigalková, M. Vrbka and V. Velebný, *J. Biomed. Mater. Res., Part B*, 2022, **110**, 2595–2611.
31 R. J. A. England, J. J. Homer, L. C. Knight and S. R. Ell, *Clin. Otolaryngol. Allied Sci.*, 1999, **24**, 67–68.
32 D. J. Kosman, *Coord. Chem. Rev.*, 2013, **257**, 210.
33 H. Xin, X. Sha, X. Jiang, L. Chen, K. Law, J. Gu, Y. Chen, X. Wang and X. Fang, *Biomaterials*, 2012, **33**, 1673–1681.
34 R. W. Korsmeyer, R. Gurny, E. Doelker, P. Buri and N. A. Peppas, *Int. J. Pharm.*, 1983, **15**, 25–35.
35 N. A. Peppas, P. Bures, W. Leobandung and H. Ichikawa, *Eur. J. Pharm. Biopharm.*, 2000, **50**, 27–46.
36 P. J. Flory, *Principles of Polymer Chemistry*, Cornell University Press, 1953.
37 M. Martini, P. S. Hegger, N. Schädel, B. B. Minsky, M. Kirchhof, S. Scholl, A. Southan, G. E. M. Tovar, H. Boehm and S. Laschat, *Materials*, 2016, **9**, 810.
38 T. Keck, R. Leiacker, H. Riechelmann and G. Rettinger, *Laryngoscope*, 2000, **110**, 651–654.
39 T. T. Hoang Thi, J. S. Lee, Y. Lee, K. M. Park and K. D. Park, *Macromol. Biosci.*, 2016, **16**, 334–340.
40 S. H. Kim, Y. H. An, H. D. Kim, K. Kim, S. H. Lee, H. G. Yim, B. G. Kim and N. S. Hwang, *Int. J. Biol. Macromol.*, 2018, **110**, 479–487.
41 T. Xing, X. Li, S. Guo, R. C. Tang, J. He Cai and S. Q. Zhou, *Text. Res. J.*, 2015, **85**, 1743–1748.
42 M. A. Maria-Solano, C. V. Ortiz-Ruiz, J. L. Muñoz-Muñoz, J. A. Teruel-Puche, J. Berna, P. A. Garcia-Ruiz and F. Garcia-Canovas, *J. Mol. Catal. B: Enzym.*, 2016, **125**, 6–15.
43 S. Tembe, S. Kulkarni, M. Karve and S. F. D'Souza, *Sens. Transducers J.*, 2009, **107**, 111–118.
44 B. Hormoz Broumand and J. Harold Smith, *J. Am. Chem. Soc.*, 1952, **68**, 1013–1016.
45 J. Lee, K. Chang, S. Kim, V. Gite, H. Chung and D. Sohn, *Macromolecules*, 2016, **49**, 7450–7459.

46 M. J. Sever and J. J. Wilker, *J. Chem. Soc., Dalton Trans.*, 2004, **4**, 1061–1072.
47 S. M. Angel, N. R. Gomer, S. K. Sharma, C. McKay and N. Ames, *Appl. Spectrosc.*, 2012, **66**, 137–150.
48 Z. Guo, K. Ni, D. Wei and Y. Ren, *RSC Adv.*, 2015, **5**, 37377–37384.
49 A. Kotzianova, J. Rebicek, O. Zidek, M. Pokorny, J. Hrbac and V. Velebny, *Anal. Methods*, 2015, **7**, 9900–9905.
50 G. Stojkov, Z. Niyazov, F. Picchioni and R. K. Bose, *Gels*, 2021, **7**, 255.
51 J. Ryu, S. Kim, I. Oh, S. Kato, T. Kosuge, A. V. Sokolova, J. Lee, H. Otsuka and D. Sohn, *Macromolecules*, 2019, **52**, 6502–6513.
52 J. Pavlacky and J. Polak, *Front. Endocrinol.*, 2020, **11**, 57, DOI: **10.3389/fendo.2020.00057**.
53 D. M. Lewis, M. R. Blatchley, K. M. Park and S. Gerecht, *Nat. Protoc.*, 2017, **12**, 1620.
54 S. W. Kim, Y. H. Bae and T. Okano, *Pharm. Res.*, 1992, **9**, 283–290.
55 R. Patwa, O. Zandraa, Z. Capáková, N. Saha and P. Sáha, *Polymers*, 2020, **12**, 2690.
56 Y. Zhao, B. Yi, J. Hu, D. Zhang, G. Li, Y. Lu and Q. Zhou, *Adv. Funct. Mater.*, 2023, **33**, 2300710.
57 W. Feng and Z. Wang, *Advanced Science*, 2023, **10**, 2303326.
58 C. S. Brazel and X. Huang, *The Cost of Optimal Drug Delivery: Reducing and Preventing the Burst Effect in Matrix Systems*, American Chemical Society, 2004, vol. 11.
59 L. Figueiredo, R. Pace, C. D'Arros, G. Réthoré, J. Guicheux, C. Le Visage and P. Weiss, *J. Tissue Eng. Regener. Med.*, 2018, **12**, 1238–1246.
60 M. S. Rehmann, K. M. Skeens, P. M. Kharkar, E. M. Ford, E. Maverakis, K. H. Lee and A. M. Kloxin, *Biomacromolecules*, 2017, **18**, 3131.
61 B. S. Spearman, N. K. Agrawal, A. Rubiano, C. S. Simmons, S. Mobini and C. E. Schmidt, *J. Biomed. Mater. Res., Part A*, 2019, **108**, 279.
62 J. K. Armstrong, R. B. Wenby, H. J. Meiselman and T. C. Fisher, *Biophys. J.*, 2004, **87**, 4259.
63 J. Patterson, R. Siew, S. W. Herring, A. S. P. Lin, R. Guldberg and P. S. Stayton, *Biomaterials*, 2010, **31**, 6772.
64 J. A. Del Olmo, L. Pérez-álvarez, V. S. Martínez, S. B. Cid, R. P. González, J. L. Vilas-Vilela and J. M. Alonso, *Gels*, 2022, **8**, 223.
65 D. S. Jones, A. D. Woolfson and A. F. Brown, *Textural, viscoelastic and mucoadhesive properties of pharmaceutical gels composed of cellulose polymers*, 1997, vol. 151.
66 M. Y. Alsedfy, A. A. Ebnalwaled, M. Moustafa and A. H. Said, *Sci. Rep.*, 2024, **14**, DOI: **10.1038/s41598-024-72577-8**.

